A Generalized Secondary Frost Heave Model

Andrew C. Fowler; William B. Krantz

SIAM Journal on Applied Mathematics, Vol. 54, No. 6. (Dec., 1994), pp. 1650-1675.

Stable URL:

http://links.jstor.org/sici?sici=0036-1399%28199412%2954%3A6%3C1650%3AAGSFHM%3E2.0.CO%3B2-F

SIAM Journal on Applied Mathematics is currently published by Society for Industrial and Applied Mathematics.

A GENERALIZED SECONDARY FROST HEAVE MODEL*

ANDREW C. FOWLER[†] AND WILLIAM B. KRANTZ[‡]

Abstract. A generalized model for secondary frost heave is developed based on the one-dimensional model of O'Neill and Miller. Secondary frost heave arises during freezing owing to cryostatic suction effects that can increase the upward water permeation to facilitate ice-lens growth and increased heave. Nondimensionalization and scaling are used to simplify the model equations and to identify a dimensionless group whose magnitude characterizes the nature of secondary frost heave in different soils. Computational problems encountered by O'Neill and Miller are avoided by recognizing the boundary layer nature of the water permeation and by reducing the frozen fringe, wherein freezing and ice-lens growth occur, to a moving planar boundary across which jump boundary conditions are prescribed. This generalized model can predict the frost heave behavior of different soils. Its predictions for the initiation time, spacing, and thickness of sequential ice lenses agree with the results of qualitative observations. This model also can be used to predict differential frost heave and hence may be able to predict the occurrence of patterned ground forms influenced by secondary frost heave.

Key words. frost heave, reactive two-phase media, frozen soil, mushy zone, ice lensing

AMS subject classification. 76S05, 76T05, 35C20, 86A99

1. Introduction. "Frost heave" refers to an uplifting of the ground surface owing to freezing of water within the soil. It is ubiquitous in regions subject to prolonged freezing temperatures. Its typical magnitude exceeds that which would result from the mere expansion of water upon freezing ($\sim 10\%$). This additional heaving arises from the freezing of water drawn upward into the soil by a mechanism of cryostatic suction, which will be discussed in a subsequent section. The water which is drawn upwards typically freezes in a series of discrete ice lenses separated by frozen soil. These can range in thickness from microscopic dimensions to several centimetres in laboratory experiments, and may be even larger in the field. A distinction is drawn in the literature between a hypothetical situation in which there is a sharp interface between frozen and unfrozen regions (termed primary frost heave), and the (observed) situation where there is a thin region of partially frozen soil, termed a frozen fringe, between frozen and unfrozen soil. This situation is that of secondary frost heave (Miller, 1978) and forms our concern in this paper. When frost heave is laterally nonuniform, it is referred to as "differential frost heave." The latter can involve random heaving or can be in the form of regularly spaced earth mounds which constitute a form of patterned ground.

Frost heave is important because its potentially large magnitude and lateral nonuniformity can cause massive damage to roads, pipelines, and structures. It can also be beneficial; indeed, it accounts in part for why 75% of the freshwater resources of the earth are stored as ice. It may also prove to be of value in providing an indicator of global climate change, since the features of some forms of patterned ground are quite sensitive to environmental conditions.

Significant progress has been made in our understanding of secondary frost heave since the seminal papers by Taber (1929), (1930) and Beskow (1935). A review of this progress has been given by Black (1991), and a review of the physics of frost heave models was given by O'Neill (1983). Much recent effort has been centered in the experimental and theoretical investigations of Miller and co-workers at Cornell, and this has culminated in the development of the so-called "rigid ice" model of secondary frost heave (O'Neill and Miller, 1985) which appears to explain many of the most prominent features of secondary frost heave. In order to understand their model, one must recognise two important features of the pore pressure in freezing soils. The first may be thought of as due to chemical effects associated with clay platelets, whereby in the presence of ice and water phases, water preferentially wets the soil particles. This leads to the existence of a thin (adsorbed) film between soil and ice, in which the excess molecular attraction between water and soil leads to an anisotropic pressure tensor, in which the lateral component $p_{\parallel}$ is less than the normal component $p_{\perp}$. The difference $p_d = p_{\perp} - p_{\parallel}$ is known as the *disjoining pressure*, and is discussed by Vignes-Adler (1977) and Gilpin (1979), among others. It can be taken as a function of the local film thickness h (with $p_d \to \infty$ as $h \to 0$), and an analysis of the local lubrication dynamics of the film allows one to determine whether or not the film thickness can go to zero. The mechanism of frost heave is then thought to occur if the film cannot close, so that as an ice front moves downwards into unfrozen soil, the soil particles are physically pushed downwards relative to the ice: or equivalently the ice moves upwards.

The resultant heave is amplified by the second important feature of the pore pressure in freezing soils, namely *cryostatic suction*. That is to say, an excess water flux upwards causes heave beyond that associated with expansion on freezing, and this flux is driven by a pressure gradient in the pore water p_w. Gold (1957) associated this pore water pressure gradient with a surface tension force at the ice-water interface, and Koopmans and Miller (1966) demonstrated that, by analogy with drying-wetting processes of unsaturated soils, one could prescribe the capillary suction $p_i - p_w$ as a function of the local volumetric water fraction W within the frozen fringe, $p_i - p_w = f(W)$, where f decreases as W increases, and depends on soil type. While the magnitude of the upward water flux (and base heave) is determined by this capillary suction, the existence of a disjoining pressure is essential in order that soil particles can be forced apart and thus allow ice lenses to form. However, the magnitude of this disjoining pressure does not affect the amount of heave, but rather the film thickness between grains.

During freezing of water-saturated soils, this results in a pressure gradient parallel to the temperature gradient which draws water upward. As more water is drawn upward and frozen, the resulting ice supports progressively more of the load on the soil; this load arises from the weight of the overlying soil and any structures on the surface. Eventually the ice pressure can support the full load, thereby permitting the soil particles to separate. This initiates the formation of an ice lens which increases in thickness as more water is drawn upward. Ice-lens growth is suppressed by continued freezing within the pores which decreases the water hydraulic conductivity of the soil. In time another ice lens will be initiated which cuts off the water flow to the ice lens above it. In this manner, the alternating layers of ice lenses and soil are created which constitute the frost heaving process.

O'Neill and Miller articulate their model by solving a set of coupled unsteady-state mass and energy conservation equations. The ice pressure, unfrozen water content, and water pressure are interrelated via the Clapeyron equation appropriately modi-

fied to include cryostatic suction effects. They solve these equations using a Galerkin finite-element algorithm. Although O'Neill and Miller's model represents a significant advance in our understanding of secondary frost heave, their numerical solution is inconvenient to use. Indeed, O'Neill and Miller (1985, p. 295) comment that *"As it now stands, the model requires a great deal of computational effort under many circumstances . . . it is possible that one might obtain results similar to those produced by this complex model using a simpler version containing its presumably essential features."* Another disadvantage of O'Neill and Miller's model is that its complexity obscures exploring some of the interesting effects associated with secondary frost heave. For example, they do not use their model to explain the markedly different behavior of clays, silts, and sands. Clays do not exhibit significant frost heave, but can heave very large loads. Silts can display very large frost heave, but this can be suppressed by moderate loading. Sands, on the other hand, seldom exhibit frost heave. The physics of secondary frost heave is not made as clear as possible because O'Neill and Miller solve their model equations in dimensional form without assessing the parametric dependence. A further shortcoming of O'Neill and Miller's model is that it is one-dimensional: as such, it cannot describe differential frost heave.

The numerical difficulties encountered by O'Neill and Miller arise in part because of the very thin frozen fringe wherein ice-lens initiation and growth occur. The boundary layer nature of the frozen fringe was recognized by Piper et al. (1988) who developed a somewhat simpler numerical solution for one-dimensional secondary frost heave. Recently Fowler (1989) developed a more systematic boundary layer analysis of the one-dimensional frozen fringe.

This brief overview provides a rationale for the research described in this paper. The scope and organization of this paper are as follows. In §2, we generalize the model of O'Neill and Miller as a basis for further work on differential frost heave. In §3, we simplify these generalized equations to facilitate their solution. Nondimensionalization and algebraic reduction of the model equations are done in §4 to ascertain the parametric dependence of secondary frost heave. In §5, an analytical solution is developed for unidirectional freezing, which is used to explain the markedly different heave behavior of different soils and to assess how the heave rate depends on the load. A special form of this analytical solution is developed for one-dimensional step freezing which is used for qualitative comparisons with laboratory experiments. Finally, the implications of this generalized model for differential frost heave are assessed. In §6, the conclusions and recommendations emanating from this study are summarized.

2. Generalized model equations. The generalized three-dimensional equations describing secondary frost heave based on the one-dimensional model of O'Neill and Miller will be developed here. These equations will be of general utility in describing differential frost heave.

2.1. Physical system. Figure 1 shows a schematic cross-section of water-saturated soil undergoing secondary frost heave. The z-coordinate is measured positive upwards from the initially undisturbed ground surface. The heaved ground surface is defined by z_s which is a function of time t. We also define a basal plane at z_b, well below the depth of maximum freezing, at which the temperature and water pressure are assumed known. The plane defined by z_f corresponds to the instantaneous frost-penetration depth, below which the soil is assumed to be saturated with unfrozen water. The plane z_l defines the bottom of the most recently formed ice lens. The region between z_f and z_l is called the "frozen fringe." Within this region, unfrozen water is being drawn up by cryostatic suction. The next ice lens will form somewhere
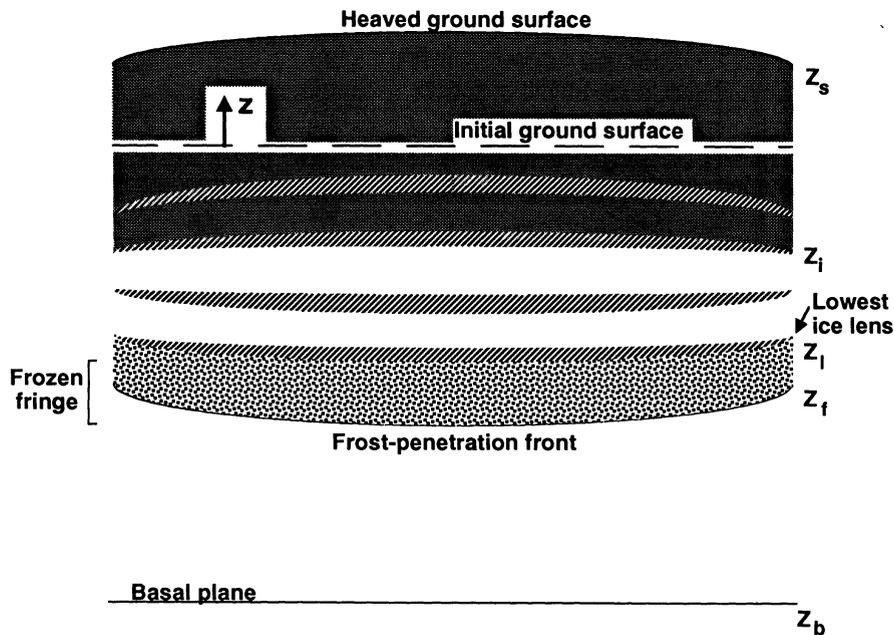
FIG. 1. *Schematic of cross-section of soil undergoing differential frost heave showing coordinate system, frozen fringe, and boundary locations.*

within the frozen fringe, at a plane at which the ice pressure can bear the entire load pressure including any virtual load owing to a subatmospheric water pressure arising from capillary pressure effects. The region above the frozen fringe consists of alternating layers of ice lenses and soil. Water permeation is not possible above the frozen fringe owing to the impermeable ice lenses. The soil above the lowest lens may still contain unfrozen water within its pores owing to the dependence of the freezing temperature on capillary suction effects. This water subsequently may freeze as cooling progresses. We define the plane z_i above which negligible freezing of pore water occurs and the unfrozen water content is nearly zero.

2.2. Energy and mass conservation equations. Now let us consider the generalized energy- and mass-conservation equations which apply above, below, and within the frozen fringe. Throughout this analysis we will assume constant physical properties. Moreover, we will assume that the thermal conductivity k and heat capacity C_p maintain the same values throughout the frozen fringe and the adjoining regions.

2.2.1. Frozen fringe. Within the frozen fringe, we have unfrozen water, ice, and energy balances given by

$$(1) \qquad W_t + \nabla \cdot \mathbf{U} = -\frac{S}{\rho_w},$$

$$(2) \qquad I_t + \nabla \cdot \mathbf{V} = \frac{S}{\rho_i},$$

$$(3) \qquad -LS + \rho C_p \frac{dT}{dt} = k \nabla^2 T$$

in which W_t and I_t denote $\partial W/\partial t$, respectively; $\mathbf{U}$ and $\mathbf{V}$ are the water permeation and ice fluxes, respectively; S (mass per unit volume per unit time) is the freezing rate; L is the heat of fusion; ρ_w, ρ_i, and ρ are the unfrozen water, ice, and overall mass densitites, respectively; and W and I are the unfrozen water and ice volume fractions, respectively, defined such that

$$(4) \qquad\qquad I + W = \phi,$$

where ϕ is the porosity of the soil which is assumed to be constant.

The temperature is given by a generalization of the Clapeyron relation, to account for the effect both of pore pressure and capillary suction on the freezing temperature

$$(5) \qquad\qquad T = T_0 \left[1 + \frac{p_w}{\rho_w L} - \frac{p_i}{\rho_i L} \right],$$

where T_0 is a reference value, p_i is the ice pressure, and p_w is the pore water pressure.

The water permeation flux $\mathbf{U}$ is assumed to be given by Darcy's law:

$$(6) \qquad\qquad \mathbf{U} = -\left(\frac{k_h}{\rho_w g} \right) \nabla[\, p_w + \rho_w g z\,]$$

in which g is the gravitational acceleration, and k_h is the hydraulic conductivity which is assumed to be given by

$$(7) \qquad\qquad k_h = k_0 \left(\frac{W}{\phi} \right)^\gamma,$$

where k_0 and γ are constants characteristic of the particular soil.

The ice flux $\mathbf{V}$ is given by

$$(8) \qquad\qquad \mathbf{V} = I\mathbf{v}_i,$$

where $\mathbf{v}_i$ is the ice velocity. Clearly if there is heaving owing to ice-lens formation, there must be a nonzero ice velocity. The ice is able to move relative to the soil, which is stationary below the lowest ice lens, via a mechanism referred to as "thermal regelation." Recall that freezing in a porous medium will result in the ice being separated from the soil particles by a thin layer of unfrozen water. If a temperature gradient is applied, this layer will freeze and thus become thinner on the cold side of a soil particle. Hence the disjoining pressure is increased there, and thus either the lateral pressure component is decreased, or the normal component is increased, or both. In fact, both must occur: the water is squeezed to the cold side by the excess lateral pressure, while the particle is squeezed in the opposite direction (i.e., up the thermal gradient) by deficit normal pressure. By this process, thermal regelation of ice past stationary soil particles can occur. O'Neill and Miller (1985) contend that if the lens and pore ice are continuously connected, then the ice velocity will be independent of the spatial coordinates and only a function of time; that is

$$(9) \qquad\qquad \mathbf{v}_i = \mathbf{v}_i(t).$$

They refer to this as the "rigid ice approximation" which they invoke in solving their one-dimensional model for secondary frost heave. The rigid ice approximation clearly has to be relaxed in order to describe differential frost heave which necessarily implies that the ice velocity depends on the spatial coordinates. In fact, there is a

misconception in O'Neill and Miller's assumption of rigid ice. While the ice itself may be rigid at any instant, its averaged velocity need not be uniform in space, since this includes both the ice motion, and that due to the regelative process, and the latter allows for a nonrigid redistribution of ice. Since ice moves down temperature gradients, an appropriate substitute for (9) might then be

$$(10) \qquad \mathbf{v}_i - \mathbf{v}_s = -\lambda \nabla T,$$

where λ is an empirical constant. An expression of just this form has been derived by Gilpin (1979). Note that the soil matrix velocity $\mathbf{v}_s$ is identically zero everywhere below the lowest ice lens where thermal regelation is occurring. Equation (10) implies that the ice velocity will not be constant unless the temperature gradient is constant; this in turn implies that even for quasi-steady-state heat transfer, there will be a jump in the ice velocity across the frozen fringe. Hence, these two models for thermal regelation will yield different results; both will be explored in this paper.

2.2.2. Region above the frozen fringe. Now let us consider the conservation equations applicable above the frozen fringe. The region between z_l and z_i in which freezing of pore water is still occurring can be shown to be quite thin. Therefore, we will ignore any latent heat effects in the energy equation above the frozen fringe, although these will be accounted for in our overall energy balance across the frozen fringe. Hence, since the ice lenses prevent permeation, only unsteady-state heat conduction is involved above the frozen fringe which is described by

$$(11) \qquad \rho C_p \frac{dT}{dt} = k \nabla^2 T.$$

2.2.3. Region below the frozen fringe. In the region below the frozen fringe, there is no freezing occurring; however, both energy transport and water permeation occur. Since the pores are saturated with unfrozen water, we have that $W = \phi$ and our unfrozen water mass balance becomes

$$(12) \qquad \nabla \cdot \mathbf{U} = 0,$$

and the energy equation is given by

$$(13) \qquad \rho C_p \frac{dT}{dt} = k \nabla^2 T.$$

2.3. Initial, boundary, and auxiliary conditions. Equations (1)–(3) and (11)–(13) then constitute the differential equations describing our secondary frost-heave model. Equations (4), (6), and (8) imply that the conservation equations can be recast in terms of three dependent variables: T, W, and p_w, for which appropriate initial and boundary conditions must be specified. In addition, we need to specify auxiliary conditions for determining the heave rate, frost-penetration velocity, and for initiating new ice lenses. We will not specify initial conditions here, since later we will show that quasi-steady-state can be assumed.

Equations (1) and (6) written for both the lower and upper fringe imply that four boundary conditions are needed for p_w. These are found from the following:

$$(14) \qquad p_i = P \quad \text{at } z = z_l,$$

$$(15) \qquad [p_w]_-^+ = 0 \quad \text{at } z = z_f,$$

$$(16) \qquad [U_n]_-^+ = 0 \quad \text{at } z = z_f,$$

$$(17) \qquad p_w = p_\infty \quad \text{at } z = z_b.$$

The notation $[\quad]_-^+$ denotes the jump across the boundary and $U_n \equiv \mathbf{U} \cdot \mathbf{n}$, in which $\mathbf{n}$ is a unit normal vector directed upward. The above introduce p_∞, the basal value of the ground-water (gauge) pore pressure, and P, the applied load (gauge) pressure; here we will ignore the weight of the soil and assume that P arises solely from a load on the surface such as some structure.

Equation (14) states that the ice pressure at the base of the lowest ice lens is equal to the load pressure. This equation is equivalent to a boundary condition on the unfrozen water pressure, since p_i and p_w are related via the cryostatic suction, which for a given soil, is

(18) $$p_i - p_w = f(W).$$

The function $f(W)$ will differ markedly depending on the soil type as illustrated in Fig. 2. Curve a represents a fine-grained, low porosity soil such as clay which can exhibit very large cryostatic suction. Curve b represents a more porous soil such as silt which displays moderate suction. Curve c represents a highly porous material such as sand which exhibits negligible suction. The difference between the curves is due to the expression of $p_i - p_w$ as $2\gamma_{iw}/r_p$, where γ_{iw} is the ice-water surface tension (about 33 mN m^{-1}) and r_p is a mean pore diameter, which can be expected to be related to grain size (Miller, 1980). Hence $p_i - p_w$ is larger for finer-grained soils, and as W is reduced so the pore diameter reduces and $p_i - p_w$ increases; it is usually considered that some unfrozen pore water remains, no matter what the suction, hence the asymptotes for the clay or silty soil.

An additional equation is needed to determine the pore-water volume fraction in (18). This is given by an overall force balance:

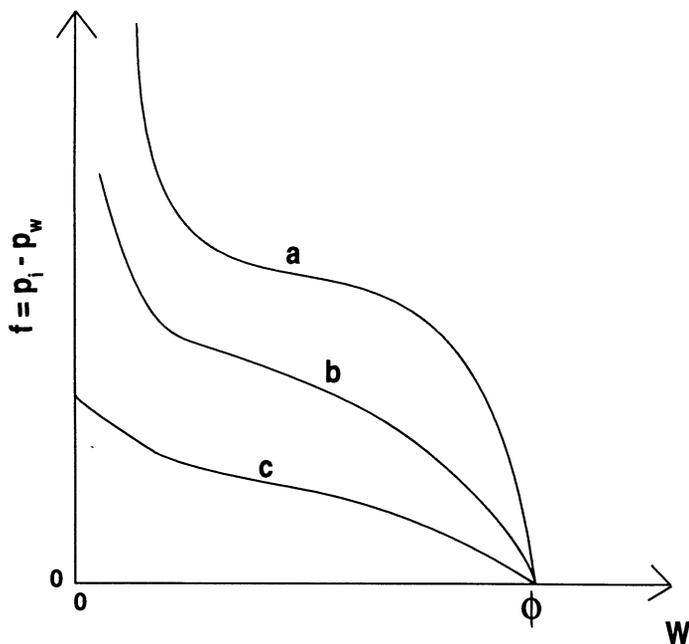(19) $$P = p_e + (1 - \chi)(p_i - p_w) + p_w = p_e + (1 - \chi)f(W) + p_w$$

FIG. 2. *Cryostatic suction* $f \equiv p_i - p_w$, *as a function of unfrozen water volume fraction, W, characteristic of* (a) —*clay,* (b) —*silt, and* (c) —*sand.*

in which p_e is the effective (absolute) pressure exerted by the soil particles when they are in contact and $\chi(W)$ is the stress-partition weighting function which might, for example, be given by

$$(20) \qquad\qquad \chi = \frac{W}{\phi},$$

although other forms are possible owing to the anisotropic nature of the water pressure tensor and to the ice/water interfacial tension; however, all forms are such that χ increases monotonically with increasing W.

   Equation (2) combined with (4) and (8) imply that one boundary condition is required for W. This is given by

$$(21) \qquad\qquad W = \phi \quad \text{at } z = z_f.$$

Equations (3), (11), and (13) imply that six boundary conditions are needed for T. These are given by the following:

$$(22) \qquad\qquad T = T_s \quad \text{at } z = z_s,$$

$$(23) \qquad\qquad T - T_0 = -\left(\frac{T_0}{\rho_i L}\right)[\delta p_w + f(W)] \quad \text{at } z = z_l,$$

$$(24) \qquad\qquad [T]_-^+ = 0 \quad \text{at } z = z_l,$$

$$(25) \qquad\qquad [T]_-^+ = 0 \quad \text{at } z = z_f,$$

$$(26) \qquad\qquad \left[\frac{\partial T}{\partial n}\right]_-^+ = 0 \quad \text{at } z = z_f,$$

$$(27) \qquad\qquad T = T_b \quad \text{at } z = z_b,$$

where $\partial/\partial n \equiv \mathbf{n} \cdot \nabla$ and

$$(28) \qquad\qquad \delta \equiv \left(1 - \frac{\rho_i}{\rho_w}\right) \sim 0.1.$$

Equation (22) represents a prescribed subfreezing temperature T_s at the ground surface. Equation (23) is the Clapeyron equation relating the freezing temperature to the unfrozen water and ice (gauge) pressures.

   Auxiliary equations are needed to determine the heave rate and the frost-penetration velocity. These are determined from overall water mass and energy balances across the frozen fringe. We will defer deriving these balances until we have simplified the description of the frozen fringe in §3.

   The above system of equations applies to the unsteady-state heat and mass transport which occur between the formation of successive ice lenses. The problem definition is completed by specifying the criterion for formation of a new ice lens. In order for ice lenses to form discretely rather than continuously, we must have $p_e \geq 0$; hence (19) implies that

$$(29) \qquad P - p_w \geq [1 - \chi(W)][p_i - p_w] = [1 - \chi(W)]f(W).$$

Figure 3 plots $p_w - P$ (solid line) and $-(1 - \chi)f(W)$ (dotted line) as functions of ν, a coordinate measured positive downward from the lowest ice lens. Both quantities decrease in magnitude with increasing ν owing to the increase in water volume fraction and decrease in disjoining pressure. Initiation of a new ice lens corresponds

to the equality in (29) or to a tangency point for the two curves in Fig. 3 shown by the vertical dashed line. Hence, our criterion for initiating a new ice lens is given by

$$(30) \qquad\qquad P - p_w = [1 - \chi(W)]f(W).$$

Other features of Fig. 3 such as the significance of the dash-dotted line will be discussed later. We also will discuss the implications of (30) for the distance between consecutive ice lenses in a subsequent section.

3. Simplification of model equations. The generalized secondary frost-heave model developed in §2 constitutes a strongly coupled nonlinear system of unsteady-state partial differential equations which precludes an analytical solution. Even its numerical solution in one dimension presents difficulties owing to the marked changes occurring within the thin frozen fringe and the complexities introduced by successive ice-lens initiation. Here we will consider appropriate simplifications of these equations which will permit analytical solutions for some cases. First, we will show that the frozen fringe is extremely thin, such that it can be represented by a moving planar boundary at which jump conditions are prescribed. Additional simplifications then will be made to facilitate evaluating the dependent variables at this moving boundary.

3.1. Thin frozen fringe. Let us first establish that the frozen fringe is very thin relative to the conduction length scale, such that it can be considered to be a moving

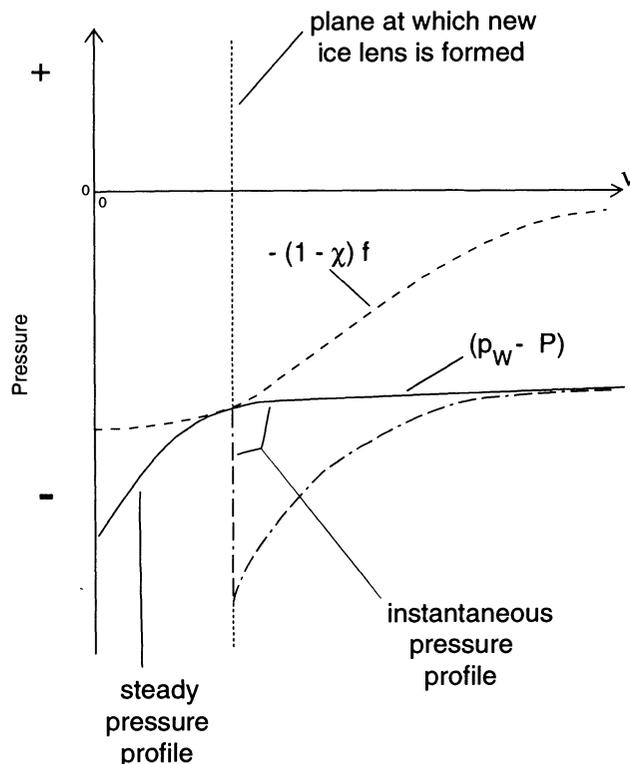FIG. 3. *Graphs of* $-(1 - \chi)f$ *and* $p_w - P$ *as functions of* v, *a coordinate measured downward from the lowest ice lens, showing the conditions for ice-lens initiation and the resulting change in the instantaneous water pressure profile.*

planar boundary. Since this is essentially a conduction process, ε, the ratio of the fringe thickness, d_f, to the characteristic depth of freezing, d, will be proportional to the respective temperature changes across these regions; that is,

$$(31) \qquad \varepsilon \equiv \frac{d_f}{d} = \frac{[T]}{\Delta T},$$

where $\Delta T \equiv T_0 - T_s$, and $[T]$ is the characteristic temperature change across the frozen fringe. The latter can be estimated by scaling the Clapeyron relation, (5), which governs the temperature within the fringe. This scaling indicates that

$$(32) \qquad [T] = \frac{\sigma T_0}{\rho L},$$

where $\sigma \sim 1$ bar is the characteristic suction in the fringe. Characteristic values for the other parameters are $T_0 \sim 300$ K and $\rho L \sim 3 \times 10^3$ bar. This implies that $[T] \sim 10^{-1}$ K. Since $\Delta T \sim 10$ K, this implies that $\varepsilon \sim 10^{-2}$. Hence, the fringe can be assumed to be a free planar boundary with respect to the frozen and unfrozen regions above and below it, respectively.

Similar scaling arguments can be used to show that the region between z_l and z_i is quite thin. This then justifies our earlier assumption that the latent heat effects occurring between z_l and z_t can be neglected in the energy equation for the region above the frozen fringe (although not in the overall energy balance used to obtain the frost-penetration velocity).

The conservation equations and boundary conditions applicable to the frozen fringe now must be expressed as jump conditions. These will serve as boundary conditions prescribed at z_f for the regions above and below the frozen fringe, and will involve evaluating dependent variables at the fringe boundaries. In order to do the latter, it is convenient to invoke several additional simplifications which are reasonable for the secondary frost-heave process. First, we will show that sensible heat advection can be ignored below the frozen line.

3.2. Negligible heat advection below fringe. There is no heat advection above the frozen fringe, since the ice lenses prevent any water permeation. For the region below the frozen fringe, a measure of the ratio of heat advection to heat conduction is the Peclet number defined by

$$(33) \qquad Pe \equiv \frac{|\mathbf{U}|d}{\kappa},$$

where $d \sim 1$ m is a characteristic freezing depth and $\kappa \sim 10^{-6}$ m^2 s^{-1} is the thermal diffusivity. The characteristic magnitude of the water permeation velocity $|\mathbf{U}|$ can be inferred from the overall water mass balance to be developed in §3.7 which suggests that $|\mathbf{U}| \sim |\mathbf{v}_i| \sim 10^{-8}$ m s^{-1}. Hence, $Pe \sim 10^{-2}$, thus implying that sensible heat advection can be ignored in (13).

3.3. Quasi-steady-state above and below fringe. The heat transfer above and below the frozen fringe can be considered to be quasi-steady-state if the conductive time scale, $t_c = d^2/\kappa \sim 10^6$ s, is much shorter than the time scale for freezing penetration, $t_f = d/|\mathbf{V}_f|$. The magnitude of the frost-penetration velocity, $|\mathbf{V}_f|$, can be inferred from the overall energy balance to be developed in §3.7 (see (56)) which suggests that $|\mathbf{V}_f| = \kappa[T]/d_f \rho_w L$. Hence, it follows that

$$(34) \qquad t_f = \frac{d^2 St}{\kappa},$$

where St is the Stefan number defined by

$$(35) \qquad St \equiv \frac{L}{C_p \Delta T}.$$

Using the characteristic values $L \sim 3 \times 10^5$ J kg^{-1}, $C_p \sim 2 \times 10^3$ J kg^{-1} K^{-1}, and $\Delta T \sim 10$ K, indicates that $St \sim 15$; thus, $t_f \sim 1.5 \times 10^7$ s. Hence, we conclude that it is reasonable to neglect the unsteady-state terms in the energy equation above and below the frozen fringe.

3.4. Negligible sensible heat effects within frozen fringe. In order to show that sensible heat effects are negligible within the frozen fringe, it is convenient to combine (1) and (3) by eliminating the freezing rate S to obtain

$$(36) \qquad \rho_w L[W_t + \nabla \cdot \mathbf{U}] + \rho C_p \frac{dT}{dt} = k \nabla^2 T.$$

The ratio of the sensible to latent heat advection terms in (36) is given by $C_p[T]/L \sim \varepsilon/St \sim 6.7 \times 10^{-4}$. Hence, sensible heat effects also may be neglected within the frozen fringe.

3.5. Permeability boundary layer within fringe. The jump boundary conditions will require the permeation flux evaluated at z_l. Hence, we need to solve the Darcy flow equation within the frozen fringe. This is facilitated by recognizing the boundary-layer nature of this flow; that is, if $\gamma \approx 9$ in (6), most of the water-pressure drop occurs within a thin boundary layer beneath the lowest ice lens. An equation for the permeation flux at z_l can be obtained by developing asymptotic approximations for W and p_w immediately beneath the lowest ice lens. Hence, let us expand W in a Taylor series about z_l:

$$(37) \qquad W = W_l + W_l' \nu + \cdots,$$

where ν again is the normal coordinate measured positive downwards from z_l, $W_l \equiv W|_{\nu=0} = W|_{z=z_l}$, and $W_l' \equiv (\partial W/\partial \nu)|_{\nu=0} = -(\partial W/\partial z)|_{z=z_l}$. Hence, to first order in ν, the water permeation flux immediately beneath the lowest ice lens can be written as follows:

$$(38) \qquad U_n \approx \frac{k_l}{\rho_w g} \left[\exp\left\langle \left(\frac{\gamma W_l'}{W_l} \right) \nu \right\rangle \frac{\partial p_w}{\partial \nu} \right],$$

where k_l is the hydraulic conductivity evaluated at z_l; that is,

$$(39) \qquad k_l = k_0 \left(\frac{W_l}{\phi} \right)^{\gamma}.$$

Since U_n varies over the length scale of the frozen fringe, d_f, whereas the water pressure varies over the permeation boundary layer thickness, d_f/γ, (38) can be integrated assuming U_n to be constant, in order to obtain an equation for the water-pressure profile within the frozen fringe:

$$(40) \qquad p_w \approx p_\infty - \frac{\rho_w g W_l U_n}{\gamma W_l' k_l} \exp\left[-\frac{\gamma W_l' \nu}{W_l} \right].$$

The above must satisfy the boundary condition given by (14). The resulting equation,

when combined with (18), then yields the desired equation for the water permeation flux at z_l:

$$(41) \qquad U_l \approx \frac{\gamma(f_l - P + p_\infty)W_l' k_l}{\rho_w g W_l},$$

where $U_l \equiv U_n|_{z_l}$, and $f_l = f(W_l)$.

3.6. Quasi-stationary profiles within the frozen fringe. The repeated initiation of new ice lenses would seem to imply that the profiles within the frozen fringe are inherently unsteady-state and incompatible with local thermodynamic equilibrium specified by the Clapeyron equation. An understanding of the nature of these transients is facilitated by Fig. 3, which illustrates the phenomenology involved in ice-lens formation. Recall that a new ice lens will be initiated at the point of tangency between the two curves in Fig. 3; see (30). Figure 3 illustrates schematically the shape of $p_w - P$ as given by (40) and (41), which arises from the value $-f_l$ at $\nu = 0$ to the asymptotic value $p_\infty - P$ as $\nu \to \infty$. To sketch $-(1 - \chi)f$, we use (37) which shows an increase of W with ν; $f(W)$ is monotone decreasing with W, while χ is increasing (e.g., if $\chi = (W/\phi)^r$, cf. O'Neill and Miller (1985)); thus $-(1 - \chi)f$ is an increasing, negative function, as illustrated by the dashed line. Since W varies on the length scale of the frozen fringe, d_f, whereas p_w varies on the length scale of the permeation boundary layer, d_f/γ, the point of tangency must occur within the permeation boundary layer where $p_w \approx p_\infty$ and $W \approx W_l$. Hence, our criterion for initiating a new ice lens becomes

$$(42) \qquad P - p_\infty \approx (1 - \chi_l)f_l$$

where $f_l \equiv f(W_l)$ and $\chi_l = \chi(W_l)$. At the initiation of a new ice lens, p_i instantaneously decreases to the load pressure P, since the pore-ice and lens-ice pressures must be continuous at z_l. This then implies that the local values of p_i, p_w, W, and T do not satisfy thermodynamic equilibrium as dictated by the Clapeyron equation. Because of the near incompressibility of water, p_w can adjust rapidly to the instantaneous values of W and T as shown by the dash-dotted line in Fig. 3. If local thermodynamic equilibrium is established on a time scale t_{eq} which is much shorter than the time scale for consecutive ice-lens formation, t_{lens}, which in turn is much shorter than the time scale for frost penetration, t_f, then the profiles within the frozen fringe can be considered to be quasi-stationary. The time scale t_f is given by (34); hence, we need to determine the time scales t_{eq} and t_{lens}.

The time scale t_{eq} is obtained by scaling (36), the energy equation within the fringe, in which the sensible heat effects now can be ignored based on §3.4:

$$(43) \qquad \rho_w L[W_t + \nabla \cdot \mathbf{U}] \approx k\nabla^2 T.$$

The second term in the above can be assessed by combining (1), (2), and (8) which yields

$$(44)$$
$$\rho_w W_t + \rho_i I_t + \nabla \cdot [\rho_w \mathbf{U} + \rho_i I \mathbf{v}_i] = \rho_w \, \delta W_t + \rho_w[\nabla \cdot \mathbf{U} + (1 - \delta)\nabla \cdot \{(\phi - W)\mathbf{v}_i\}] = 0.$$

Hence, (44) implies that $\nabla \cdot \mathbf{U} \approx -\nabla \cdot \{(\phi - W)\mathbf{v}_i\}$. The scale for the conduction term in (43) is obtained from the Clapeyron relation, (23). Hence, the energy equation within the fringe can be written in the following form:

$$(45) \qquad \rho_w L[W_t - \nabla \cdot \{(\phi - W)\mathbf{v}_i\}] \approx -\frac{kT_0}{\rho_i L} \nabla \cdot [\delta \nabla p_w + \nabla f(W)].$$

A measure of the latent heat terms in the above is $\rho_w L[W]/t_{eq}$, whereas a measure of the conduction terms is given by $kT_0 \, \delta\sigma\gamma^2/\rho_i L d_f^2$, where $[W]$ is a measure of the change in W which occurs within the permeation boundary layer. The latter can be assessed from (37) which indicates that

(46)
$$[W] = W - W_l \approx W_l'\nu \approx W_l' \frac{d_f}{\gamma} \sim \gamma^{-1}.$$

Hence, since $\delta\gamma \sim O(1)$, the time scale t_{eq}, obtained by balancing the latent heat with the conduction terms in (45) is given by

(47)
$$t_{eq} \sim \rho_w L \left(\frac{\rho_i L}{kT_0 \sigma}\right) \frac{d_f^2}{\gamma^2} = \left(\frac{\varepsilon}{\gamma^2}\right)\left(\frac{d^2 St}{\kappa}\right).$$

The time scale for initiation of consecutive ice lenses is given by

(48)
$$t_{lens} \sim \frac{(d_f/\gamma)}{|\mathbf{V}_f|} \sim \left(\frac{\varepsilon}{\gamma}\right)\left(\frac{d^2 St}{\kappa}\right).$$

Hence, we conclude that $t_{eq} \ll t_{lens} \ll t_f$, which justifies assuming that the profiles within the frozen fringe are quasi-stationary.

3.7. Jump boundary conditions at frozen fringe. Equations (43) and (44) are of the general form

(49)
$$\psi_t + \nabla \cdot \mathbf{f} = 0.$$

Conservation equations of this form, when integrated across a thin region, lead to jump conditions expressed as

(50)
$$[\psi]_-^+ V_n = [f_n]_-^+,$$

where $V_n \equiv \mathbf{V} \cdot \mathbf{n}$ and $f_n \equiv \mathbf{f} \cdot \mathbf{n}$, provided there is no surface source.

We will use the above formalism to complete the description of our generalized secondary frost-heave model. This requires collapsing the frozen fringe to a plane at which appropriate jump boundary conditions are specified. In addition, it requires developing equations to determine the heave rate, $v_s \equiv v_i^+ \equiv v_{in}|_{z_l^+} = \mathbf{v}_i \cdot \mathbf{n}|_{z_l^+}$, and the frost-penetration rate, $V_f \equiv \mathbf{V}_f \cdot \mathbf{n}$. The notation z_l^+ denotes evaluation on the ice-lens side of z_l, as opposed to the frozen fringe side which will be denoted by z_l^-. This notation allows for the fact that variables such as U_n, W, $\partial T/\partial n$, and v_{in} experience discontinuities across z_l. In particular, v_{in} will be discontinuous across z_l if the rigid ice approximation is not invoked.

Note that the frost-penetration rate, V_f, is not a smooth function of time, since the position of the lowest ice lens moves downwards in jumps. However, since t_{lens}, the time scale for successive lens initiation, is much shorter than t_f, the time scale for frost penetration, we can assume that V_f changes smoothly in time on the larger t_f scale.

Applying the formalism indicated by (50) to (44) and (43) then yields

(51)
$$\left[\rho_w W + \rho_i(\phi - W)\right]_{z_f}^{z_l^-} V_f = \left[\rho_w U_n + \rho_i(\phi - W)v_{i_n}\right]_{z_f}^{z_l^-},$$

(52)
$$\rho_w L[U_n - W V_f]_{z_f}^{z_l^-} = \left[k \frac{\partial T}{\partial n}\right]_{z_f}^{z_l^-}.$$

Equation (51) determines $U_f \equiv U_n|_{z_f}$ if the quantities W_l, V_f, $U_l \equiv U_n|_{z_l^-}$, and $v_i^- \equiv v_{i_n}|_{z_l^-}$ are known. Equation (52) determines $\partial T / \partial n|_{z_l^-}$ if the additional quantity $\partial T / \partial n|_{z_f}$ is known. The latter is determined from (26) and the solution to the energy equation below the frozen fringe. Additional equations now need to be developed to determine the remaining quantities.

Equation (42) gives W_l directly. Equation 41 determines U_l if the quantities f_l and W_l' are known. Equation (18) gives f_l directly once W_l is determined; that is

$$(53) \qquad f_l = P - p_l = f(W_l).$$

The quantity W_l' can be obtained by differentiating the Clapeyron relation given by (23) to obtain

$$(54) \qquad \left.\frac{\partial T}{\partial n}\right|_{z_l^-} = -\left(\frac{T_0}{\rho_i L}\right)\left[\delta \frac{\partial p_w}{\partial n} + \frac{\partial f}{\partial n}\right]_{z_l^-} = \left(\frac{T_0}{\rho_i L}\right)\left[\delta \frac{\partial p_w}{\partial v} + f_l' W'\right]_{z_l^-},$$

where $f_l' \equiv \partial f/\partial W|_{z_l^-}$ is determined by differentiating (18) with respect to W. The quantity $\partial p_w/\partial v|_{z_l^-}$ can be obtained by combining (38) and (41). The resulting form of (54) then is

$$(55) \qquad \left.\frac{\partial T}{\partial n}\right|_{z_l^-} = \left(\frac{T_0 W_l'}{\rho_i L}\right)\left[\frac{\delta\gamma(f_l - P + p_\infty)}{W_l} + f_l'\right].$$

Equation (55) then gives W_l' in terms of previously determined quantities.

An independent equation for determining the frost-penetration rate, V_f, can be obtained from a jump energy balance across the thin region between z_f and z_i. Note that by including the thin region between z_l and z_i, this jump energy balance includes the latent heat effects associated with freezing of pore water above the lowest ice lens as well as water drawn into the lowest ice lens. This jump energy balance then yields

$$(56) \qquad \rho_w L[U_n - WV_f]_{z_f}^{z_i} = k\left[\frac{\partial T}{\partial n}\right]_{z_f}^{z_i}$$

Equation (56) constitutes the Stefan condition for this moving boundary problem; it gives the frost-penetration rate V_f in terms of previously determined quantities. Note that $\partial T / \partial n|_{z_i}$ is obtained from the solution to the energy equation above z_i.

The quantity v_i^- is related to the heave rate, $v_s \equiv v_i^+$, via a water mass balance across z_l given by

$$(57) \qquad \rho_w U_l + \rho_i(\phi - W_l)v_i^- = \rho_i v_i^+ = \rho_i v_s$$

For the rigid ice approximation, (9) implies that

$$(58) \qquad v_i^- = v_i^+ = v_s$$

and (57) gives the heave rate directly in terms of U_l. For the alternate thermal regelation model based on Gilpin's work, (10) implies that

$$(59) \qquad v_i^- = -\lambda \left.\frac{\partial T}{\partial n}\right|_{z_l^-}$$

Equation (59) when combined with (57) then gives the heave rate v_s in terms of previously determined quantities. Note that (57) implies that there is a discontinuity in the temperature gradient across z_l; this arises owing to the latent heat effects associated with freezing of the water permeating to the lowest ice lens. Moreover,

note that latent heat effects associated with the freezing of pore water above the frozen fringe imply that $\partial T/\partial n|_{z_f^+} \neq \partial T/\partial n|_{z_i}$.

The description of our generalized secondary frost-heave model is now complete. This model consists of the quasi-steady-state energy equation, which must be solved above and below the frozen fringe, subject to boundary conditions at the ground surface and basal plane, along with jump conditions at the freezing front z_f. The latter constitute two boundary conditions expressed in terms of nine interrelated equations. In the next section, the model equations will be nondimensionalized and the nine equations required to specify the jump conditions at z_f will be reduced to two equations to be solved for the frost-penetration rate, V_f, and heave rate, v_s.

4. Nondimensionalization and reduction. In order to obtain the minimum parametric representation for this secondary frost-heave model, let us nondimensionalize the describing equations using the following dimensionless variables:

(60)
$$T^* \equiv \frac{T - T_0}{\Delta T}, \quad x^* \equiv \frac{x}{d}, \quad V_f^* \equiv \frac{V_f}{[U]}, \quad v_i^* \equiv \frac{v_i}{[U]},$$
$$U_l^* \equiv \frac{U_l}{[U]}, \quad v_s^* \equiv \frac{v_s}{[U]}, \quad t^* \equiv \frac{t}{[t]}$$

in which $d \equiv -z_b$ is the conduction length scale. Equation (56) combined with the definition of the Stefan number given by (35) suggests that

(61)
$$[U] = \frac{\kappa}{dSt}.$$

The implicit time dependence enters through solving the equations for V_f and v_s to obtain the frost-penetration depth z_f and the heaved ground-surface location z_s; hence, we define the convective time scale as follows:

(62)
$$[t] = d/[U].$$

The capillary suction as well as the other pressure variables appearing in the describing equations are nondimensionalized by σ, a characteristic value of the cryostatic suction; that is,

(63)
$$f^* \equiv \frac{f(W)}{\sigma}.$$

Let us now eliminate the variables U_l, U_f, W_l', p_l, $\partial T/\partial n|_{z_f^-}$, and v_i^- from (41), (51)–(53), and (55)–(57), and introduce the above dimensionless variables in order to obtain the following two dimensionless equations (in which the superscript * has been dropped with the understanding that the variables v_s, V_f, G_i, and G_f are now dimensionless):

(64)
$$\dot{V}_f = \frac{\left[1 + \delta - (1 + \tilde{\beta})(\phi - W_l)\eta\right]G_i - (1 + \tilde{\beta})G_f}{\delta W_l + \phi + \tilde{\beta}(\phi - W_l) - \eta(1 + \tilde{\beta})(\phi - W_l)W_l},$$

(65)
$$v_s = -\alpha[G_i - W_l V_f],$$

where $G_t \equiv \partial T/\partial n|_{z_t}$, $G_f \equiv \partial T/\partial n|_{z_f}$, and the dimensionless parameter $\tilde{\beta}$ is defined by

(66)
$$\tilde{\beta} = \beta_l \left[\frac{f_l - N}{-W_l f_l' - \delta\gamma(f_l - N)} \right],$$

where N is the dimensionless load defined by

$$(67) \qquad N \equiv \frac{P - p_\infty}{\sigma}.$$

The dimensionless parameter β_l in equation (66) is characteristic of the particular soil type and is defined by

$$(68) \qquad \beta_l \equiv \frac{\gamma \rho_i L^2 k_l}{g k T_0}.$$

The definition of the dimensionless parameters η and α depends on which thermal regulation model is invoked. For the rigid ice assumption of O'Neill and Miller

$$(69) \qquad \eta \equiv \frac{\tilde{\beta}(1 + \delta)}{(1 + \tilde{\beta})(1 - \phi + W_l)},$$

$$(70) \qquad \alpha = \eta,$$

whereas for the thermal regulation model based on Gilpin's work

$$(71) \qquad \eta \equiv \frac{\mu}{(1 + \tilde{\beta})},$$

$$(72) \qquad \alpha \equiv \frac{\tilde{\beta}(1 + \delta) + \mu(\phi - W_l)}{(1 + \tilde{\beta})},$$

where the dimensionless parameter μ is defined by

$$(73) \qquad \mu \equiv \frac{\lambda L \rho_w}{k}.$$

Equation (64) is the dimensionless Stefan condition at z_f. It is essentially like an ordinary Stefan condition, except that the heat flux from below is enhanced by the factor proportional to $\tilde{\beta}$, which is a measure of the importance of heat advection by the incoming water flux. Equation (65) can be solved for the heave velocity v_s once the frost-penetration rate V_f is known. However, (70) and (72) indicate that the heave rate predicted by the two thermal regelation models can differ markedly for small values of $\tilde{\beta}$, unless μ is very small as well.

In order to assess the magnitude of dimensionless parameters, typical values of the dimensional parameters are given in Table 1: The value of the empirical constant λ was determined from the work of Gilpin (1979). The values of the hydraulic conductivity were obtained from Freeze and Cherry (1979). Table 1 indicates that the characteristic values of β_l for the three soil types considered here are

$$(74) \qquad \beta_l \sim c(W_l/\phi)^\gamma,$$

where $c = c_a \sim 10^{-1} - 10$ for clay, $c = c_b \sim 10^2 - 10^4$ for silt, $c = c_c \sim 10^7 - 10^9$ for sand. We see that β_l is very sensitively dependent on W_l, and hence on N. Taking a representative value of $W_l/\phi = 0.5$, so $(W_l/\phi)^\gamma \sim 10^{-3}$, we thus have

$$(75) \qquad \begin{aligned} \beta_l &\sim 10^{-4} - 10^{-2} \ll 1 && \text{(clay)}, \\ \beta_l &\sim 10^{-1} - 10 \sim 1 && \text{(silt)}, \\ \beta_l &\sim 10^4 - 10^6 \gg 1 && \text{(sand)}. \end{aligned}$$

TABLE 1
Typical parameter values

Parameter	Symbol	Typical Value
ice density	ρ_i	0.9×10^3 kg m^{-3}
water density	ρ_w	1×10^3 kg m^{-3}
heat of fusion	L	3×10^5 J kg^{-1}
thermal conductivity	k	2 W m^{-1} K^{-1}
heat capacity	C_p	2 kJ kg^{-1} K^{-1}
temperature scale	ΔT	10 K
hydraulic conductivity exponent	γ	7–9
porosity	ϕ	0.4
water volume fraction	W_l	0.2
gravitational acceleration	g	10 m s^{-2}
freezing temperature	T_0	273 K
pressure scale	σ	1 bar
Gilpin model constant	λ	10^{-10} m^2 s^{-1} K^{-1}
hydraulic conductivity	k_0	$10^{-12} - 10^{-10}$ m s^{-1} (clay)
		$10^{-9} - 10^{-7}$ m s^{-1} (silt)
		$10^{-4} - 10^{-2}$ m s^{-1} (sand)

We shall see that β_l is a type of critical parameter which characterizes the nature of secondary frost heave in different soil types.

The typical parameter values in Table 1 indicate that $\mu \approx 10^{-2}$. This suggests that the heave velocities predicted by the two different thermal regelation models obtained by substituting either (70) or (72) into (65) can differ markedly for fine-grained soils such as clays which are characterized by very small values of β_l.

5. Results and discussion. In this section we first will develop an analytical solution for one-dimensional frost penetration which will permit us to assess the principal features of secondary frost heave in different soil types. We then will consider a special form of this solution for one-dimensional step-freezing which allows a qualitative comparison with laboratory experiments on secondary frost heave. Finally, we will discuss the implications of the generalized secondary frost-heave model developed here for differential frost heave.

5.1. One-dimensional frost penetration. For one-dimensional frost penetration, our simplified secondary frost-heave model requires a solution to the following differential equation:

$$(76) \qquad \frac{\partial^2 T}{\partial z^2} = 0, \qquad z_f < z < z_s, \qquad z_b < z < z_f.$$

The dimensionless boundary conditions are given by the following:

$$(77) \qquad\qquad\qquad T = -1 \quad \text{at } z = z_s,$$

$$(78) \qquad\qquad\qquad [T]_-^+ = 0 \quad \text{at } z = z_f,$$

$$(79) \qquad\qquad\qquad T = 0 \quad \text{at } z = z_f,$$

$$(80) \qquad\qquad\qquad T = \theta_b \quad \text{at } z = z_b,$$

where again the superscript * on the dimensionless variables has been dropped to simplify the notation, and the dimensionless temperature θ_b is defined by

$$(81) \qquad\qquad\qquad \theta_b \equiv \frac{T_b - T_0}{T_0 - T_s}.$$

The solution to the above system of equations written in dimensionless form is given by

$$(82) \qquad T = -1 + \frac{(z_s - z)}{(z_s - z_f)}, \qquad z > z_f,$$

$$(83) \qquad T = \theta_b \left[\frac{(z_f - z)}{(z_f - z_b)} \right], \qquad z < z_f.$$

The above solutions then provide the quantities $G_i \equiv \partial T/\partial n|_{z_i}$ and $G_f \equiv \partial T/\partial n|_{z_f}$ in (64) and (65). The resulting dimensionless equations for the frost-penetration rate and heave rate then are given by

$$(84) \qquad V_f = \frac{dz_f}{dt} = -\frac{A}{z_s - z_f} + \frac{B}{z_f - z_b},$$

$$(85) \qquad v_s = \frac{dz_s}{dt} = \alpha \left[\frac{1}{z_s - z_f} + W_l V_f \right],$$

where

$$(86) \qquad A \equiv \frac{(1 + \delta) - (1 + \tilde{\beta})(\phi - W_l)\eta}{\delta W_l + \phi + \tilde{\beta}(\phi - W_l) - \eta(1 + \tilde{\beta})(\phi - W_l)W_l},$$

$$(87) \qquad B \equiv \frac{(1 + \tilde{\beta})\theta_b}{\delta W_l + \phi + \tilde{\beta}(\phi - W_l) - \eta(1 + \tilde{\beta})(\phi - W_l)W_l}.$$

A similar description of one-dimensional secondary frost heave in terms of two coupled ordinary differential equations was obtained by Piper et al. (1988). However, they did not invoke jump conditions across the frozen fringe and therefore had to solve a somewhat more complicated problem numerically. Moreover, the parameter $\tilde{\beta}$ is not explicit in their model and must be determined via iteration in their numerical solution.

Equations (84) and (85) can be recast as a linear system via the following variable transformations:

$$(88) \qquad h_1 \equiv z_s - z_f, \quad h_2 \equiv z_f - z_b, \quad \frac{dt}{d\tau} \equiv h_1 h_2.$$

Equations (84) and (85) then assume the following form:

$$(89) \qquad \frac{dh_2}{d\tau} = -Ah_2 + Bh_1,$$

$$(90) \qquad \frac{dh_1}{d\tau} = [A + \alpha(1 - AW_l)]h_2 - B(1 - \alpha W_l)h_1.$$

The above equations can be solved explicitly for h_1, h_2, and t in terms of exponential functions of τ, subject to appropriate initial conditions for z_s and z_f. This appears to be the first closed-form analytical solution developed to describe secondary frost heave. It would be of interest to compare the predictions of this simplified model with those of the numerical solution of O'Neill and Miller (1985). However, this is not quantitatively possible at present owing to insufficient details on the numerical algorithm and input parameters used by O'Neill and Miller. The form of (85) provides

considerable information on the nature of frost heave in different soil types. Note that this equation indicates that the heave rate is directly proportional to the dimensionless parameter α. The influence of the load and soil type on α enters through the parameters W_l and $\tilde{\beta}$ appearing in the definition of α given either by (70) or (72) corresponding to the two thermal regelation models being considered here. These two equations imply that

(91) $\alpha \approx \tilde{\beta}$ when $\tilde{\beta} \ll 1$ for (70),

(92) $\alpha \approx \mu$ when $\tilde{\beta} \ll 1$ for (72),

(93) $\alpha \approx 1$ when $\tilde{\beta} \gg 1$ for both (70) and (72).

Hence, the influence of the load and soil type on the heave rate is directly related to their effect on the parameter $\tilde{\beta}$, which enters through the parameters W_l, $f_l - N$, and f'_l appearing in the definition of $\tilde{\beta}$ given by (66). Let us now examine how the load and soil type affect each of these parameters appearing in $\tilde{\beta}$.

The influence of load and soil type on W_l is determined from (42) which shows that W_l is a monotonically decreasing function of increasing load. Define the saturation S at the lowest lens as

(94) $S = W_l / \phi,$

and choose the representative functions f and χ as

(95) $f = \dfrac{(1 - S)^p}{S^q}, \qquad \chi = S^r,$

where we expect $0 < p < 1$, $q \geq 0$, $r > 0$. S as a function of N is then determined from

(96) $\dfrac{(1 - S^r)(1 - S)^p}{S^q} = N,$

and is depicted in Fig. 4.

Since the heaving parameter $\alpha \sim \tilde{\beta}/(1 + \tilde{\beta})$, and $\tilde{\beta} \sim cS^\gamma$, we see that α decreases rapidly with applied load. The heave rate is modulated by the square-
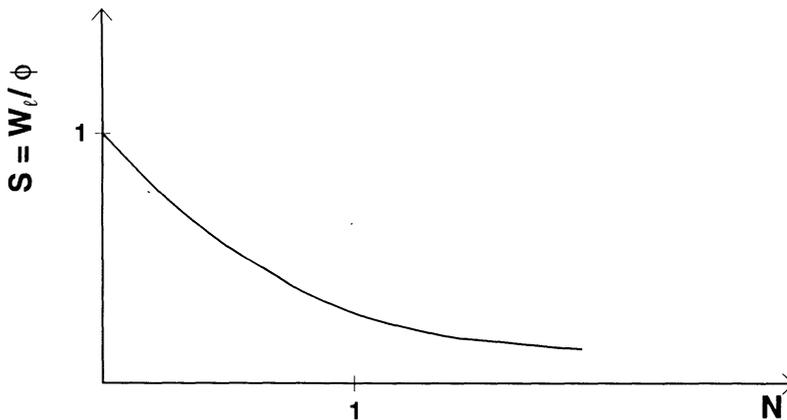

FIG. 4. *Variation of saturation $S = W_l / \phi$ with load N.*

bracketed term in (66), which can be written as β_m, where

$$(97) \qquad \beta_m = \frac{1}{(W_l/\chi_l)\{\ln(1/f_l)\}' - \delta\gamma}.$$

For the choices χ and f in (95), this gives

$$(98) \qquad \beta_m = \frac{1}{qS^{-r} + pS^{-(r-1)}/(1-S) - \delta\gamma},$$

whose behaviour depends on the sizes of p, q, δ and γ. In Fig. 5 we plot the typical behaviour of β_m as a function of N, using (96). Fig 5(a) is appropriate for $q > q_c$ $(= \{\sqrt{p} + \sqrt{\delta\gamma}\}^2$ for $r = 1)$, and may be appropriate to clay-rich soils, while Fig. 5(b) is appropriate for $q < q_c$, and may be expected for sandy soils. The right-hand dashed portion of Fig. 5(b) is absent if $q = 0$ i.e., $f(0)$ is finite (e.g., for sands) but in any case is irrelevant, since we see that when $\beta_m \to \infty$, then W_l' becomes large. In this case the approximation which determines W_l in (42) becomes inaccurate. The dotted portion is then inapplicable. A more accurate calculation shows that a terminal lens forms, and the model breaks down. Similarly, the approximation becomes invalid as $W_l' \to 0$, i.e., $\beta_m \to 0$. This is practically irrelevant since the dimensionless unsaturated effective pressure $N = (P - p_\infty)/\sigma$ will be nonzero (and in reality depends on the porosity ϕ).

In Fig. 6, we indicate schematically our results for heave rate. We have put a vertical line at a nominal value $N = N_0 > 0$ corresponding to zero load. There is a nominal association between soil type and the behaviour of β_m, and Fig. 6 represents the situation where we suppose sand and silt have β_m as in Fig. 5(b) (low and medium p, q) while clay has the behaviour of Fig. 5(a). If the p, q values for silt are higher than those for sand, then the corresponding N value $(N = N_c)$ where $\beta_m \to \infty$ is higher. Then Fig. 6 is consistent with the statements: sands do not generally heave $(N_0 > N_c)$; silts heave a lot, but only small loads $(N < N_c)$; clays heave slowly, but indefinitely large loads. Obviously these conclusions are malleable, but are consistent with the overall observations. The dotted portions of the curves are unreliable, as the approximation in (42) breaks down, and the overall trend is a decrease in heave rate with increasing load.

5.2. Step-freezing analysis. Let us now consider the implications of the frost heave model developed here for step-freezing experiments in which a soil initially at a uniform temperature is suddenly subjected to a constant subfreezing surface temperature. Experiments of this type have been used by Tabor (1929), (1930), Feldman (1988), and others to study the characteristic thickness and spacing of ice lenses in frost heave. The general observations are that the ice-lens thickness increases monotonically and that the ice-lens spacing increases to a constant value as the freezing front penetrates further into the soil.

We will consider step-freezing in a clay for which $\alpha \approx \bar{\beta} \ll 1$, thus implying that z_s is quite small relative to z_b and z_f. Hence, (84) and (85) simplify to the following:

$$(99) \qquad V_f = \frac{dz_f}{dt} \approx \frac{A}{z_f} + \frac{B}{z_f + 1},$$

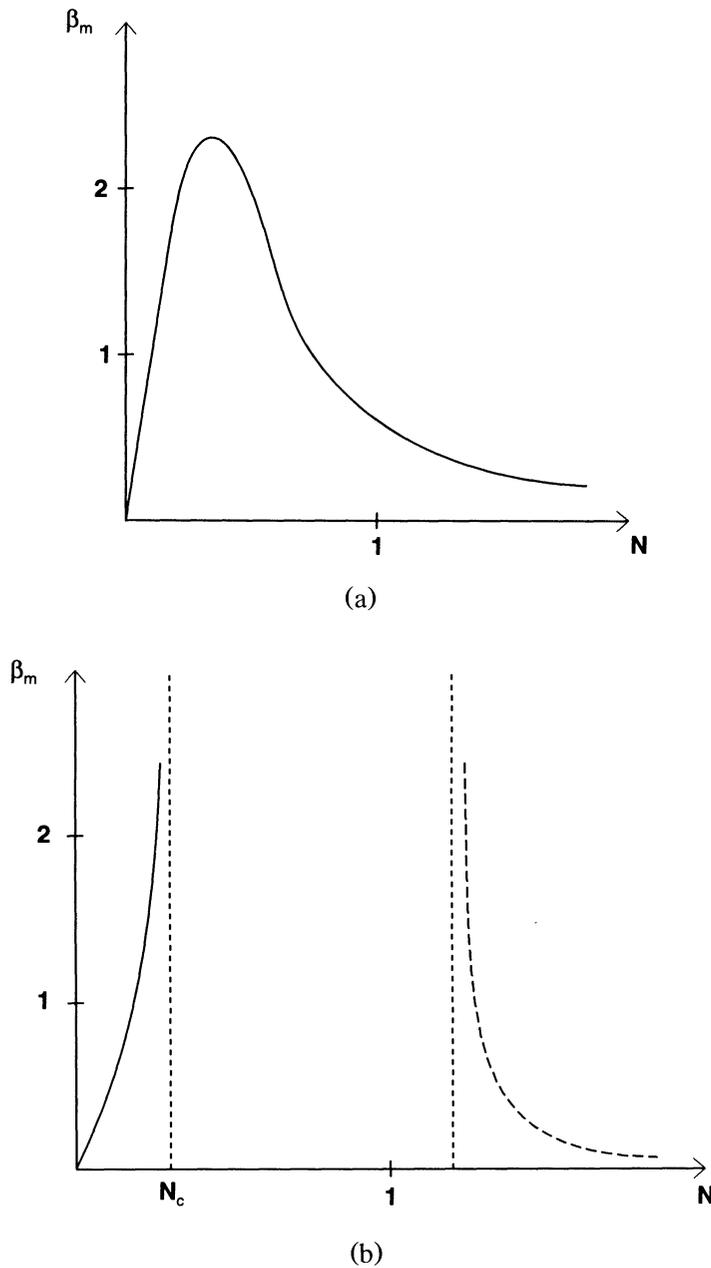$$(100) \qquad v_s = \frac{dz_s}{dt} \approx -\alpha\left[\frac{1}{z_f} - W_t\frac{dz_f}{dt}\right].$$

FIG. 5. *Variation of* β_m *defined by* (98) *with* N (a) *clay-type soil*; (b) *silt or sand type.*

The initial conditions for step-freezing are $z_f = z_s = 0$. Note that the above equations are nondimensionalized using the dimensionless variables defined by (60), where the superscript * has been dropped.

A general solution to (99) can be obtained; however, in order to elucidate the physics more clearly we will develop asymptotic solutions for very short and very large
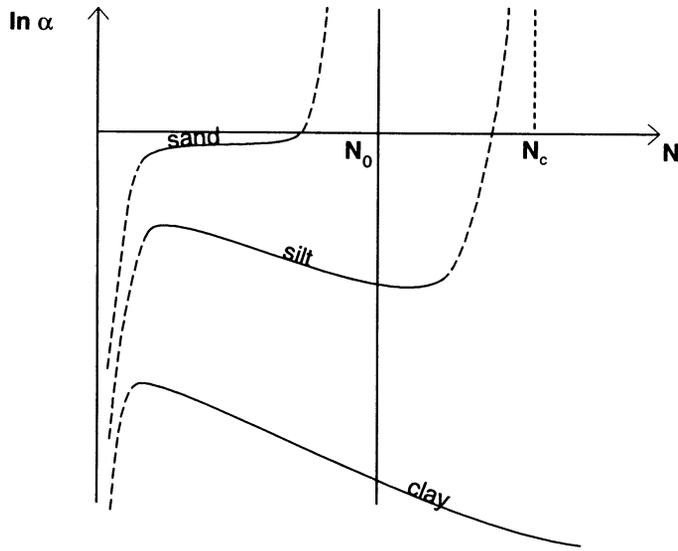
FIG. 6. *Schematic heave rates for clay, silt, and sand.*

times. For very small values of z_f, the solutions to the above equations are given by

$$(101) \qquad z_f \approx (2At)^{1/2},$$

$$(102) \qquad z_s \approx -\alpha(1 - AW_l)\left[\frac{2t}{A}\right]^{1/2},$$

which correspond to similarity solutions at small times. The corresponding solutions for the frost-penetration rate and heave velocity are given by

$$(103) \qquad V_f \approx \left(\frac{A}{2t}\right)^{1/2},$$

$$(104) \qquad v_s \approx -\frac{\alpha(1 - AW_l)}{(2At)^{1/2}}.$$

At very large times, $dz_f/dt \rightarrow 0$. Hence, the solutions to (99) and (100) are given by

$$(105) \qquad z_f \rightarrow -\frac{A}{A + B} \approx -\frac{1}{1 + \theta_b},$$

$$(106) \qquad z_s \rightarrow \left[\frac{A + B}{A}\right]\alpha t \approx (1 + \theta_b)\alpha t.$$

The corresponding solutions for the frost-penetration rate and heave velocity are given by

$$(107) \qquad V_f \approx 0$$

$$(108) \qquad v_s \approx \alpha\left(\frac{A + B}{A}\right) \approx \alpha(1 + \theta_b)$$

These solutions for short and long times appear to agree with the numerical solution of O'Neill and Miller (1985) both functionally (the $t^{1/2}$ and t behaviour is similar) and quantitatively, although a precise comparison with experimental studies is not possible owing to a lack of relevant data used in the earlier experiments. Numerical solutions of (84) and (85) have been given by Fowler and Noon (1993).

   We now seek to use the asymptotic solutions developed above in order to infer the thickness and spacing of the ice lenses. The scaling analyses in §§3.1 and 3.6 imply that d_l, the dimensionless spacing between consecutive ice lenses, is given by

$$(109) \qquad d_l \approx \frac{\varepsilon K}{\gamma}(\alpha/v_s),$$

where K is a complicated function of W_l, and is $O(1)$. This result can be obtained for d_l by determining the distance from the lowest ice lens at which the slopes of the quantities $p_w - P$ and $-[1-x]f$ are equal within the fringe (i.e., see Fig. 3). If t_l^n is the time at which the nth ice lens is initiated, then the time between initiation of consecutive ice lenses, $t_l = t_l^n - t_l^{n-1}$, is determined from the following:

$$(110) \qquad \int_{t_l^{n-1}}^{t_l^n} |V_f|\, dt = d_l.$$

If $t_l^n - t_l^{n-1}$ is very small, then the frost penetration rate V_f is approximately constant between the formation of consecutive ice lenses and t_l is given by

$$(111) \qquad t_l \approx \frac{d_l}{|V_f|}.$$

The local ice-lens thickness h_l is given by

$$(112) \qquad h_l = \int_{t_l^{n-1}}^{t_l^n} |v_s|\, dt.$$

If $t_l^n - t_l^{n-1}$ is very small, then the heave rate is approximately constant between the formation of consecutive ice lenses and h_l is given by

$$(113) \qquad h_l \approx |v_s| t_l.$$

   Let us consider the behavior of d_l, t_l, and h_l at short frost-penetration times. Equation (109) indicates that the spacing between consecutive ice lenses, d_l, increases in time since from equation (107), $d_l \propto (\alpha/v_s) \sim t^{1/2}$. The behavior of t_l and h_l at short times can be obtained by substituting (103) and (104) into (111) and (113). We then conclude the following secondary frost heave behavior for short frost-penetration times:

$$(114) \qquad d_l \sim (\epsilon/\gamma)t^{1/2},$$

$$(115) \qquad t_l \approx d_l\left(\frac{2t}{A}\right)^{1/2},$$

$$(116) \qquad h_l \approx \frac{\alpha(1 - AW_l)d_l}{A}.$$

That is, for short frost-penetration times, the interlens spacing, time of formation, and local ice-lens thickness all increase with increasing time. These predictions are in agreement with step-freezing experiments.

At very long frost-penetration times, $V_f \rightarrow 0$, thus implying that z_f becomes constant. Equation (109) then implies that d_l becomes constant as well. The behavior of t_l and h_l at long times can be obtained by substituting (107) and (108) into equations (110) and (112). The following behavior then is inferred for very long frost-penetration times:

(117) $$d_l \rightarrow (\epsilon K/\gamma)(-z_f),$$

(118) $$t_l \rightarrow \infty,$$

(119) $$h_l \approx \alpha(1 + \theta_b)t_l \rightarrow \infty.$$

That is, for very long frost-penetration times, the interlens spacing tends to a constant and the time of formation as well as the local ice-lens thickness tends to infinity. This predicted behavior also is observed during step-freezing experiments.

5.3. Differential frost heave. Thus far we have considered the implications of our generalized model for the special case of one-dimensional (nondifferential) secondary frost heave. This generalized model also can describe three-dimensional (differential) secondary frost heave. In this case one must solve the quasi-steady-state form of Laplace's equation for the temperature subject to boundary conditions given by (77)–(80) and the Stefan and heave conditions given by (64) and (65). The solution to the differential frost-heave problem is beyond the scope of this paper. However, we can provide some discussion on how the one-dimensional equations must be developed in order to provide insight into differential frost heave.

It can be shown that the generalized secondary frost-heave model developed here contains a potential instability mechanism whereby differential frost heave can occur. This instability mechanism might explain the striking regularity of some forms of patterned ground such as earth hummocks which are known to be accompanied by secondary frost heave (see Krantz et al. (1988) and Krantz (1990).

In the case of differential frost heave, an additional equation is needed to relate the deformation of the frozen soil to the stress acting on it. It is reasonable to assume that the soil remains incompressible, that the frozen region above z_f behaves elastically, and that the elastic strains respond quasi-statically to lens production. A tractable model for small variations in the local heave rate based on thin shell theory is given by

(120) $$\frac{\partial P}{\partial t} = Ev_i,$$

where E is a dimensionless group which is proportional to the modulus of elasticity. More complex models could certainly be used, although information on the required material properties may be difficult to obtain. In addition, the O'Neill–Miller prescription of ice velocity as $v_i = v_i(t)$ is no longer viable, and must be replaced by a different model such as Gilpin's equation (59).

6. Conclusions. In this paper we have generalized the one-dimensional secondary frost heave model of O'Neill and Miller to describe differential frost heave. We have achieved considerable simplification while retaining the essential features of O'Neill and Miller's model by nondimensionalizing and scaling the describing equations in order to asses the principal terms. This scaling indicated why O'Neill and Miller commented that solving their model equations required a "... *great deal of computational effort...*". The frozen fringe, wherein all the active freezing and ice-lens formation occur, is quite thin. Moreover, the pressure drop which drives the

water permeation within the fringe is confined to an extremely thin boundary layer. A computational scheme which does not recognize these two features of secondary frost heave necessarily will be quite inefficient and difficult to implement. We averted these difficulties by using proper asymptotics to describe the permeation boundary layer and by reducing the frozen fringe to a moving planar boundary across which jump boundary conditions are prescribed.

The nondimensionalization indicated that secondary frost heave is characterized by one dimensionless parameter, namely β_l defined by (68). The markedly different secondary frost heave behavior of clays, silts, and sands can be explained solely in terms of this parameter.

The generalized model developed here is amenable to an analytical solution which appears to describe all the principal features of step-freezing experiments. It predicts the gradual increase in the time required to initiate consecutive ice lenses and in the thickness of subsequent ice lenses. It also predicts that the interlens spacing initially increases and eventually become constant. These predictions are in agreement with step-freezing experiments.

Our model provides considerable insight into the coupled mechanisms operative in secondary frost heave. We see that the latter arises because of cryostatic suction effects which can cause upward permeation of additional water which contributes to ice-lens growth. The cryostatic suction increases with decreasing unfrozen water content because of the increasing curvature of the water-ice interface. The functional relation between the suction and unfrozen water content is characteristic of the particular soil. Sands, silts, and clays display a progressively more marked increase in suction with decreasing water content. An increase in load causes a decrease in the unfrozen water content as dictated by the Clapeyron relation and thereby an increase in the suction. However, an increase in load also makes it more difficult to initiate a new ice lens since a larger disjoining pressure, and hence suction, is required to cause separation of the soil grains. The implications of these two opposing effects of an increase in load are that new ice lenses are initiated most easily for clays, which exhibit secondary frost heave under nearly all load conditions, but are rarely seen in sands. The magnitude of frost heave depends on the hydraulic conductivity, which is smallest for clays and largest for sands. For this reason, clays exhibit relatively small heave. The largest frost heave is exhibited by silts which can display significant suctions while maintaining reasonably large permeation rates.

An interesting potential application of our generalized model is to the study of spatial instabilities of secondary frost heave. The generalized equations developed here provide a framework for exploring this instability mechanism which is of considerable interest since it may describe forms of patterned ground known to be influenced by differential frost heave.

Further studies of secondary frost heave should be directed toward considering more complex soil behavior allowing for elastic deformation and compressibility of the soil. The model developed here also can be extended to incorporate solutal effects on the freezing temperature and the influence of nonsaturated soils on secondary frost heave.

REFERENCES

G. BESKOW (1935), *Soil freezing and frost heaving with special application to roads and railroads*, The Swedish Geological Society, C, no. 375, Year Book no. 3, (J. O. Osterberg, transl.).

P. BLACK (1991), *Historical perspective of frost heave research*, Historical Perspectives in Frost Heave Research: the Early Works of S. Taber and G. Beskow, P. B. Black and M. J. Hardenberg, eds., CRREL special report 91-23, CRREL, Hanover, NH, pp. 3–7.

G. M. FELDMAN (1988), *Formation problem of thick ice streaks, ice saturated horizons in permafrost*, Proc. Fifth Int. Conf. Permafrost. K. Senneset, ed., Tapir, Trondheim, pp. 339–343.

A. C. FOWLER, (1989), *Secondary frost heave in freezing soils*, SIAM J. Appl. Math., 49, pp. 991–1008.

A. C. FOWLER, AND C. G. NOON (1993), *A simplified numerical solution of the Miller model of secondary frost heave*, Cold Reg. Sci. Tech., 21, pp. 327–336.

R. A. FREEZE, AND J. A. CHERRY (1979), Groundwater, Prentice-Hall, Englewood Cliffs, NJ.

R. R. GILPIN, (1979), *A model of the "liquid-like" layer between ice and a substrate with applications to wire regelation and particle migration*, J. Colloid Interface Sci., 68, pp. 235–251.

———— (1980), *A model for the prediction of ice lensing and frost heave in soils*, Water Resour. Res., 16, pp. 918–930.

W. B. KRANTZ, K. J. GLEASON, AND N. CAINE (1988), *Patterned ground*, Sci. Am., 259, pp. 68–76.

L. W. GOLD, (1957), *A possible force mechanism associated with freezing of water in porous materials*, High. Res. Board Bull., 168, pp. 65–72.

R. W. R. KOOPMANS, AND R. D. MILLER (1966), *Soil freezing and soil water characteristic curves*, Soil Sci. Soc. Am. Proc., 30, pp. 680–685.

W. B. KRANTZ, (1990), *Self organization manifest as patterned ground in recurrently frozen soils*, Earth- Sci. Rev., 29, pp. 117–130.

R. D. MILLER, (1978), *Frost heaving in non-colloidal soils*, Proc. Third Int. Conf. Permafrost, Edmonton, Canada. N.R.C., Ottawa, Canada, pp. 708–713.

———— (1980), *Freezing phenomena in soils*, in Applications of soil physics, D. Hillel, ed., Academic Press, New York, pp. 254–299.

K. O'NEILL, (1983), *The physics of mathematical frost heave models: a review*, Cold Reg. Sci. Tech., 6, pp. 275–291.

K. O'NEILL, AND R. D. MILLER (1985), *Exploration of a rigid ice model of frost heave*, Water Resource. Res., 21, pp. 281–296.

D. PIPER, J. T. HOLDEN AND R. H. JONES (1988), *A mathematical model of frost heave in granular materials*, Proc. Fifth Int. Conf. Permafrost, K. Senneset, ed., Tapir, Trondheim, pp. 370–376.

S. TABER, (1929), *Frost heaving*, J. Geol., 37, pp. 428–461.

———— (1930), *The mechanics of frost heaving*, J. Geol., 38, pp. 303–317.

M. VIGNES-ADLER, (1977), *On the origin of the water aspiration in a freezing dispersed medium*, J. Colloid Interface Sci., 60, pp. 162–171.